Air Force Institute of Technology

AFIT Scholar

12-1-2012

Dual-arm Z-scan Technique to Extract Dilute Solute Nonlinearities from Solution Measurements

Manuel R. Ferdinandus
Air Force Institute of Technology

Matthew Reichert
University of Central Florida

Trenton R. Ensley
University of Central Florida

Honghua Hu
University of Central Florida

Dmitry A. Fishman
University of Central Florida

See next page for additional authors

Recommended Citation

Manuel R. Ferdinandus, Matthew Reichert, Trenton R. Ensley, Honghua Hu, Dmitry A. Fishman, Scott Webster, David J. Hagan, and Eric W. Van Stryland, "Dual-arm Z-scan technique to extract dilute solute nonlinearities from solution measurements," Opt. Mater. Express 2, 1776-1790 (2012).

Authors

Manuel R. Ferdinandus, Matthew Reichert, Trenton R. Ensley, Honghua Hu, Dmitry A. Fishman, Scott Webster, David J. Hagan, and Eric W. Van Stryland

Dual-arm Z-scan technique to extract dilute solute nonlinearities from solution measurements

Manuel R. Ferdinandus, Matthew Reichert, Trenton R. Ensley, Honghua Hu, Dmitry A. Fishman, Scott Webster, David J. Hagan, and Eric W. Van Stryland*

CREOL, The College of Optics and Photonics, University of Central Florida, Orlando, FL, 32816, USA
*ewvs@creol.ucf.edu

Abstract: We present a technique in which small solute nonlinearities may be extracted from large solvent signals by performing simultaneous Z-scans on two samples (solvent and solution). By using a dual-arm Z-scan apparatus with identical arms, fitting error in determining the solute nonlinearity is reduced because the irradiance fluctuations are correlated for both the solvent and solution measurements. To verify the sensitivity of this technique, the dispersion of nonlinear refraction of a squaraine molecule is measured. Utilizing this technique allows for the effects of the solvent n_2 to be effectively eliminated, thus overcoming a longstanding problem in nonlinear optical characterization of organic dyes.

OCIS codes: (190.0190) Nonlinear optics; (190.4400) Nonlinear optics, materials; (190.4710) Optical nonlinearities in organic materials.

References and links

1. M. A. Bader, G. Marowsky, A. Bahtiar, K. Koynov, C. Bubeck, H. Tillmann, H.-H. Hörhold, and S. Pereira, "Poly(p-phenylenevinylene) derivatives: new promising materials for nonlinear all-optical waveguide switching," J. Opt. Soc. Am. B **19**(9), 2250–2262 (2002).
2. D. N. Christodoulides, I. C. Khoo, G. J. Salamo, G. I. Stegeman, and E. W. Van Stryland, "Nonlinear refraction and absorption: mechanisms and magnitudes," Adv. Opt. Photonics **2**(1), 60–200 (2010).
3. M. Lipson, "Guiding, modulating, and emitting light on silicon – challenges and opportunities," J. Lightwave Technol. **23**(12), 4222–4238 (2005).
4. C. Koos, P. Vorreau, T. Vallaitis, P. Dumon, W. Bogaerts, R. Baets, B. Esembeson, I. Biaggio, T. Michinobu, F. Diederich, W. Freude, and J. Leuthold, "All-optical high-speed signal processing with silicon-organic hybrid slot waveguides," Nat. Photonics **3**(4), 216–219 (2009).
5. Z.-M. Meng, F. Qin, and Z.-Y. Li, "Ultrafast all-optical switching in one-dimensional semiconductor-polymer hybrid nonlinear photonic crystals with relaxing Kerr nonlinearity," J. Opt. **14**(6), 065003 (2012).
6. B. J. Eggleton, B. Luther-Davies, and K. Richardson, "Chalcogenide photonics," Nat. Photonics **5**, 141–148 (2011).
7. J. S. Aitchison, A. Villeneuve, and G. I. Stegeman, "All-optical switching in a nonlinear GaAlAs X junction," Opt. Lett. **18**(14), 1153–1155 (1993).
8. T. Tanabe, M. Notomi, S. Mitsugi, A. Shinya, and E. Kuramochi, "All-optical switches on a silicon chip realized using photonic crystal nanocavities," Appl. Phys. Lett. **87**(15), 151112 (2005).
9. J. M. Hales, J. Matichak, S. Barlow, S. Ohira, K. Yesudas, J.-L. Brédas, J. W. Perry, and S. R. Marder, "Design of polymethine dyes with large third-order optical nonlinearities and loss figures of merit," Science **327**(5972), 1485–1488 (2010).
10. J. M. Hales, S. Zheng, S. Barlow, S. R. Marder, and J. W. Perry, "Bisdioxaborine polymethines with large third-order nonlinearities for all-optical signal processing," J. Am. Chem. Soc. **128**(35), 11362–11363 (2006).
11. B. Esembeson, M. L. Scimeca, T. Michinobu, F. Diederich, and I. Biaggio, "A high-optical quality supramolecular assembly for third-order integrated nonlinear optics," Adv. Mater. **20**(23), 4584–4587 (2008).
12. M. Kivala and F. Diederich, "Acetylene-derived strong organic acceptors for planar and nonplanar push-pull chromophores," Acc. Chem. Res. **42**(2), 235–248 (2009).
13. C. Zhan, D. Zhang, D. Zhu, D. Wang, Y. Li, D. Li, Z. Lu, L. Zhao, and Y. Nie, "Third- and fifth-order optical nonlinearities in a new stilbazolium derivative," J. Opt. Soc. Am. B **19**(3), 369–375 (2002).
14. M. Sheik-Bahae, A. A. Said, T.-H. Wei, D. J. Hagan, and E. W. Van Stryland, "Sensitive measurement of optical nonlinearities using a single beam," IEEE J. Quantum Electron. **26**(4), 760–769 (1990).
15. H. Ma, S. L. Gomes, and C. B. de Araujo, "Measurements of nondegenerate optical nonlinearity using a twocolor single beam method," Appl. Phys. Lett. **59**(21), 2666–2668 (1991).

16. Q.- Gong, J.- Li, T.- Zhang, and H. Yang, "Ultrafast third-order optical nonlinearity of organic solvents investigated by subpicosecond transient optical Kerr effect," Chin. Phys. Lett. **15**(1), 30–31 (1998).
17. S. Couris, M. Renard, O. Faucher, B. Lavorel, R. Chaux, E. Koudoumas, and X. Michaut, "An experimental investigation of the nonlinear refractive index (n_2) of carbon disulfide and toluene by spectral shearing interferometry and z-scan techniques," Chem. Phys. Lett. **369**(3-4), 318–324 (2003).
18. R. Dawley, Sales Department, Starna Cells, Inc., P.O. Box 1919, Atascadero, CA, 93423 (personal communication, 2012).
19. S. Webster, D. Peceli, H. Hu, L. A. Padilha, O. V. Przhonska, A. E. Masunov, A. O. Gerasov, A. D. Kachkovski, Y. L. Slominsky, A. I. Tolmachev, V. V. Kurdyukov, O. O. Viniychuk, E. Barrasso, R. Lepkowicz, D. J. Hagan, and E. W. Van Stryland, "Near-unity quantum yields for intersystem crossing and singlet oxygen generation in polymethine-like molecules: design and experimental realization," J. Phys. Chem. Lett. **1**(15), 2354–2360 (2010).
20. A. Savitzky and M. J. E. Golay, "Smoothing and differentiation of data by simplified least squares procedures," Anal. Chem. **36**(8), 1627–1639 (1964).
21. OriginLab (2012). Origin (version 8.6.0) [Computer software]. Northampton, MA. Retrieved June 1, 2012. Available from http://www.OriginLab.com.
22. D. Milam, "Review and assessment of measured values of the nonlinear refractive-index coefficient of fused silica," Appl. Opt. **37**(3), 546–550 (1998).
23. J. Ward, "Calculation of nonlinear optical susceptibilities using diagrammatic perturbation theory," Rev. Mod. Phys. **37**(1), 1–18 (1965).
24. B. J. Orr and J. F. Ward, "Perturbation theory of the non-linear optical polarization of an isolated system," Mol. Phys. **20**(3), 513–526 (1971).
25. M. Balu, L. A. Padilha, D. J. Hagan, E. W. Van Stryland, S. Yao, K. Belfield, S. Zheng, S. Barlow, and S. Marder, "Broadband Z-scan characterization using a high-spectral-irradiance, high-quality supercontinuum," J. Opt. Soc. Am. B **25**(2), 159–165 (2008).
26. P. N. Butcher and D. Cotter, *The Elements of Nonlinear Optics* (Cambridge University Press, 1990).
27. R. L. Sutherland, *Handbook of Nonlinear Optics* (Marcel Dekker, 1996).
28. B. Gu, W. Ji, and X.-Q. Huang, "Analytical expression for femtosecond-pulsed Z scans on instantaneous nonlinearity," Appl. Opt. **47**(9), 1187–1192 (2008).
29. R. A. Ganeev and I. A. Kulagin, "Single-shot Y-scan for characterization of the nonlinear optical parameters of transparent materials," J. Opt. A, Pure Appl. Opt. **11**(8), 085001 (2009).
30. K. Kamada, "Mechanisms of ultrafast refractive index change in organic system," Proc. SPIE **4797**, 65–75 (2003).

1. Introduction

The rapid development of applications for photonic switching has led to aggressive efforts to find materials with large optical nonlinearities [1–3]. To this end, many different types of materials have been extensively studied [4–8], with organic materials having been identified as being particularly promising due to their ease of processing and large nonlinear figures of merit [9–13]. Here we are primarily interested in Kerr-like nonlinear refraction, where the irradiance-dependent refractive index is given by $n(I) = n_0 + n_2 I$ where n_0 and n_2 are the linear and nonlinear refractive indices, respectively, and I is the irradiance. One of the quickest and most efficient means of characterizing organics has been to study their optical properties in solutions by using such methods as the Z-scan technique which can simultaneously measure nonlinear absorption (NLA) and nonlinear refraction (NLR) utilizing a single Gaussian beam [14]. In this technique, as shown in Fig. 1(a), the sample is scanned along the axis of a focusing beam, while measuring the transmittance $T(Z)$ through an aperture in the far field. As described in [14], NLR results in self-lensing, causing changes in the far field beam radius, so that the aperture transmittance is sensitive to NLR. Removal of the aperture causes the Z-scan to be only sensitive to NLA, in which case, we refer to the Z-scan as an "open-aperture" (OA) Z-scan, and the transmittance will be a symmetric function of Z, where $Z = 0$ is defined at the beam waist (shown in Fig. 1(b)) and $q_0 = \alpha_2 I_0 L$ describes the transmission loss due to two-photon absorption (2PA) where α_2 is the 2PA coefficient, I_0 is the peak irradiance, and L is the sample thickness as detailed in [14]. Usually, we normalize $T(Z)$ to unity for the sample position far from the beam waist, where the irradiance is low and the nonlinear effects are negligible. In the absence of NLA, $T(Z)$ for the closed-aperture (CA) scan will be an antisymmetric function of Z showing a peak in transmittance prior to focus and a valley after focus for a negative n_2, with the order of the peak and valley being reversed for a positive n_2. In the case where NLA coexists with NLR, the CA Z-scan exhibits features due to both NLA

and NLR, as can be seen from the closed aperture scan in Fig. 1(b). However, it is found that dividing the OA scan by the CA scan (CA/OA) yields a result, that is similar to that which would have been obtained for pure NLR (see Fig. 1(b)). In addition to the sample arm for CA Z-scans, a reference arm (Fig. 1(a)) in the same geometry as the sample arm with a matching closed aperture is used to reduce the noise [15].

In the case of pure NLR (or for the divided result when small NLA is present), the difference between the peak and valley of $T(Z)$, ΔT_{p-v} is directly proportional to the induced nonlinear phase shift $\Delta\phi_0$ (for small $\Delta\phi_0$ [14]) and hence to n_2, i.e. from [14] $\Delta T_{p-v} \approx 0.406(1-S)^{0.25}\Delta\phi_0$, in the absence of linear absorption where S is the linear transmittance of the aperture and $\Delta\phi_0 = k_0 n_2 I_0 L$, $k_0 = 2\pi/\lambda$ is the free space wavenumber where λ is the wavelength. Typically, a $\Delta T_{p-v} \sim 1\%$ corresponds to a nonlinearly induced phase shift in the center of the Gaussian beam of $\sim\lambda/250$. This interferometric sensitivity can be understood by noting the input beam induces a phase mask in the sample near focus, which has the greatest nonlinear phase shift ($\Delta\phi_0$) at the center of the beam, while the wings of the beam propagate linearly through the sample (i.e. $\Delta\phi_0 \to 0$). This induced phase mask in the sample near focus alters the propagation of the beam to the far field, causing the redistribution of the irradiance at the closed aperture, i.e. diffraction, which can be thought of as interference between the wings of the beam and the center of the beam.
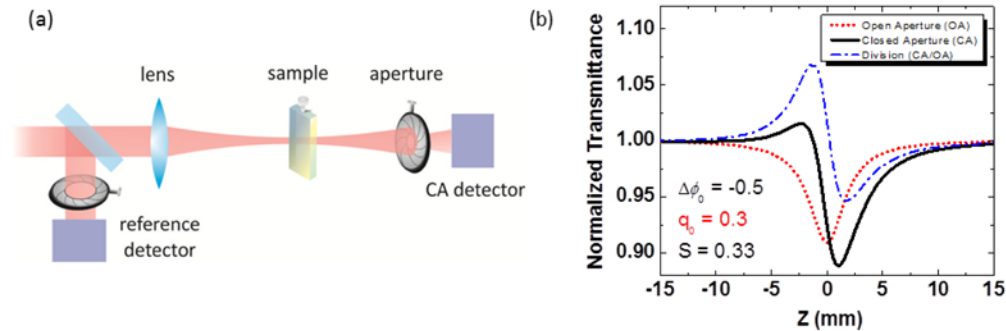

Fig. 1. (a) The Z-scan experimental apparatus and (b) Z-scan open aperture (OA, red dotted line) and closed aperture (CA, black solid line) signals along with division (CA/OA, blue dot-dash line) for $\Delta\phi_0 = -0.5$, $S = 0.33$, and $q_0 = 0.3$.

When measuring the nonlinear properties of molecules in solution, the NLA of the solvent is usually small and determination of α_2 for the solute is not problematic. However this is not the case for NLR. Typically, the NLR per molecule of the solvent is much less than that of the solute, but the large density of solvent molecules yields a large net NLR that may dominate the signal due to the solute. Additionally, there is a contribution to the measured n_2 due to the cells used to hold the samples. In cases where the n_2 of the solute is small, large discrepancies can arise when reporting the nonlinearity of the solute since the NLR of the solvent and cells must be subtracted from that of the solution. Thus, the determination of solute nonlinearities in regions where the NLR is similar to or much smaller than the solvent or cells has been difficult.

To determine the NLR of a solute in solution, typically two sequential Z-scans are performed, one for the solution and one for the solvent. Each Z-scan curve is individually fit to determine the nonlinear refractive index for the solution, $n_{2,S}$ and the solvent, $n_{2,V}$, separately. These values are then subtracted to yield the nonlinear refractive index of the solute, $n_{2,U}$. Literature values for solvents cannot be used since there is a wide range of values reported using different techniques. For example, Gong et al. [16] reported a value of 2.2×10^{-15} cm^2/W at 820 nm for toluene using the optical Kerr effect, while Couris et al. [17] reported a value of 0.88×10^{-15} cm^2/W and 1.3×10^{-15} cm^2/W at 800 nm for toluene using spectral shearing interferometry and Z-scan, respectively. Subtracting a literature value for

$n_{2,V}$ from $n_{2,S}$ could lead to varying values of $n_{2,U}$; therefore, it is essential to measure the solvent at each time a nonlinear measurement is made to avoid such large discrepancies.

Cases where $n_{2,U}$ is much smaller than $n_{2,S}$ are often of interest. For example, a molecule designed for use in thin films may have low solubility, but may need to be characterized in solution. Also, in characterizing the frequency dependence of the nonlinear response, there may be regions where the NLR changes sign, so that $n_{2,U}$ is inevitably small. To resolve these problems, we note that a significant source of the noise in a closed aperture Z-scan is due to laser beam fluctuations. In subtracting two separate Z-scans, this noise cannot be eliminated because the noise in the two sequential scans is uncorrelated. However, if the two Z-scans (for solvent and solution, respectively) are taken simultaneously using identical Z-scan arms, as shown in Fig. 2, much of the noise (energy fluctuations, pointing instabilities, etc…) is correlated between the two arms and hence this noise will be eliminated upon subtraction, leaving only the uncorrelated noise (detector amplifier noise, air currents, etc…). This assumes that the measured solution normalized transmission $T_S(Z)$ is the sum of the solvent normalized transmission $T_V(Z)$ and the solute normalized transmission $T_U(Z)$ (see appendix). This expands upon the work of Ma et al. [15], where a reference arm with a focusing lens and aperture matched to the signal arm was used to increase the signal-to-noise ratio. While using a reference arm with no sample goes part way toward correlating the noise, including a solution reference in the second arm and doing Z-scan simultaneously (i.e. dual-arm Z-scan) does a considerably better job to further remove the correlated noise as confirmed in the experiments reported here.

In this work, we carefully prepare the dual Z-scan arms to be as similar to each other as possible by using matched optics and equal arm path lengths and pulse energies to give equal irradiances. This correlates the noise in both Z-scans due to laser pulse energy variation, beam pointing instability, etc., thus enhancing the signal-to-noise ratio (SNR) for determining $n_{2,U}$ By performing simultaneous Z-scans on the two arms: one arm with the solution and the second arm with only the solvent, we find that we can accurately extract $n_{2,U}$ from typically large solvent NLR signals. This allows us to determine solute nonlinearities up to an order of magnitude smaller than that without using this procedure.

2. Experimental setup

The experimental configuration is shown in Fig. 2. A Ti:Sapphire laser system (Clark-MXR, CPA 2110), with a pulse energy output of approximately 1 mJ and a pulse width of ~150 fs (FWHM), operating at a 1 kHz repetition rate, is used to pump an optical parametric generator/amplifier (Light Conversion, Ltd., TOPAS-C) which generates a wide range of wavelengths for nonlinear optical characterization. The output beam is passed through a half-wave plate and polarizer (not shown) to provide attenuation, then spatially filtered and collimated to obtain a Gaussian beam. Approximately 10% of the energy is split off by a beam sampler (not shown) used to monitor the input energy. The remaining 90% is evenly split between two arms (Arm A and Arm B) using a 50/50 dielectric beam splitter. On one of the arms (here arm B in Fig. 2), a continuously variable neutral density (ND) filter is introduced for energy equalization, which will be discussed later.
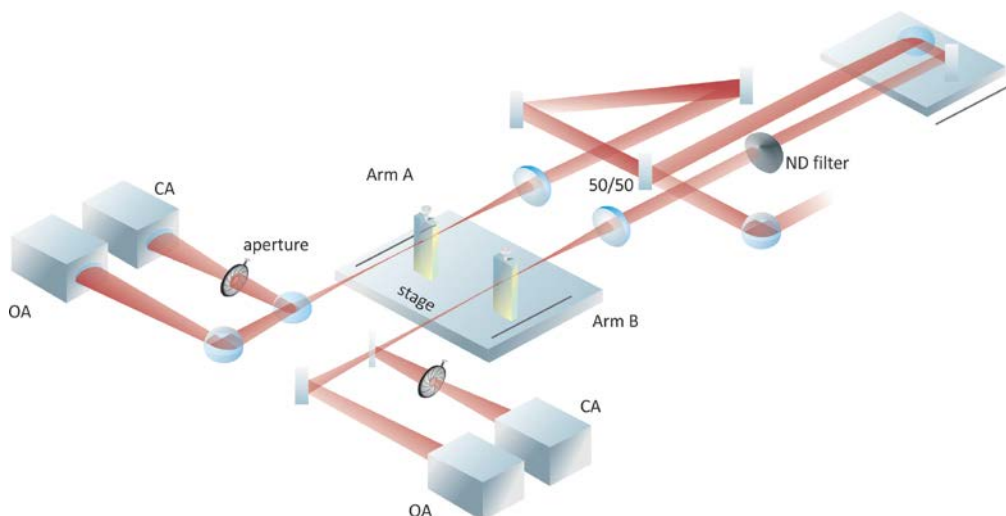
Fig. 2. Schematic of dual-arm Z-scan. The items labeled CA and OA represent the closed aperture and open aperture detectors for each arm, respectively. The reference beam used for energy monitoring is not shown.

In order to ensure that the signal from the solvent can be properly removed, it is essential that the two arms be equalized. This requires that the pulse width, beam waist, pulse energy, relative Z-position of the two samples, aperture linear transmittance, and distance from each sample to its respective aperture are matched. In addition to matching the irradiance parameters, the equipment in each arm is also matched, i.e. photodetectors, sample cuvettes matched to within tight tolerances (path length of 1 mm, matched to within 1 micron) [18], and corresponding matched optics.

The pulse widths in both arms will be identical so long as the dispersion in the optical components is the same in each arm. This is typically not a problem for pulse widths greater than 100 fs (FWHM), as in our experiments. However, for shorter pulses path differences due to the beam splitter and the ND filter used to match the energies on both arms may cause pulse widths to differ. In such cases a compensator plate in one arm should be used to account for this.

Matching the beam waists is done by collimating the beam prior to the first beam splitter, using matched optics in each arm, and equalizing the arm path lengths. To ensure that signal fluctuations due to pointing instability of the laser are correlated between the arms, the number of mirror reflections beyond the 50/50 beam splitter shown in Fig. 2 is matched so that any asymmetries in the beam profile are clipped in the same manner by the apertures placed after the samples.

Once the beam waists and pulse widths along each arm have been equalized, the pulse energy can then be equalized. Attempts to do so using energy meters failed as the accuracy is not sufficient for our purposes. Instead this was accomplished by scanning two cells filled with the same solvent, preferably with large NLR, e.g. carbon disulfide (CS_2), and attenuating one of the beams using the continuously variable ND filter until ΔT_{p-v} on each arm is equal. To ensure that the two samples experience the same irradiance and noise simultaneously at all points along the Z-axis, the relative Z-position of the samples is adjusted until the CA signals from both arms lie directly on top of each other. When subtracting the two curves from each arm, the resultant signal should yield a curve whose nonlinear effects are minimized to below the noise floor as discussed in the conclusion. This can be checked by increasing the pulse energy and verifying that the resultant signal does not change. More information on the equalization methodology is given in the appendix.
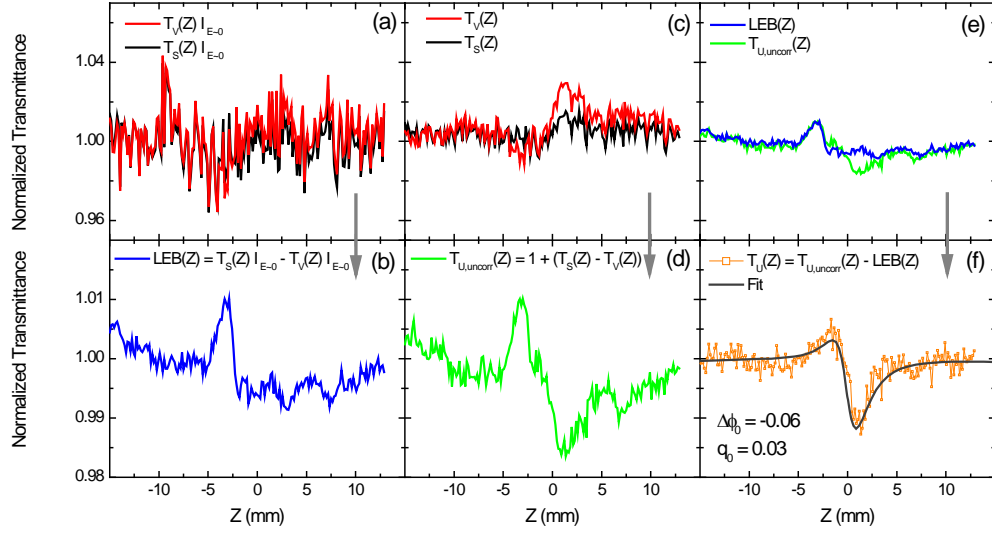
Fig. 3. Procedure of processing dual-arm Z-scan data using the low-energy background (*LEB(Z)*) and the corresponding Z-scan curves of the solution and solvent at 695nm at (a) low energy (< 1 nJ) scan of a squaraine solution (SD-O 2405 [19]) in toluene at a concentration (*C*) of 47 µM and solvent and their (b) subtraction, (c) high energy (11 nJ, I_0 = 18 GW/cm^2) scan of solution and solvent and their (d) subtraction, (e) direct comparison of (b) and (d), and (f) corrected solute signal and fit with $\Delta\phi_0$ = −0.06, q_0 = 0.03, using S = 0.33.

Once the difference between CA signals of both arms has been minimized, the cells used for alignment are replaced with cells containing the solution in one arm and the solvent in the other arm. Following Fig. 3, a scan is performed at a low irradiance (typically less than 2 GW/cm^2 in our experiments using 1 mm cells), where the nonlinear signal from either arm is less than the noise level, to correct for any remaining systematic differences in the arms due to linear effects such as cell mismatch (Fig. 3(a)). This is similar to the procedure of background subtraction described in [14]. The subtraction of the solvent CA signal $T_V(Z)$ from the solution CA signal $T_S(Z)$ at this low energy yields a signal that we refer to as the Low Energy Background *LEB(Z)* (Fig. 3(b)), which is the residual signal due to linear differences between the two arms. This is primarily due to variations in linear transmittance and/or inhomogeneities of the two cells. The *LEB(Z)* can be minimized by using a set of high quality matched cells whose manufacturing tolerances have been tightly controlled as mentioned previously.

$$LEB(Z) = T_S(Z)\big|_{E\approx 0} - T_V(Z)\big|_{E\approx 0} \qquad (1)$$

We have found that smoothing the *LEB(Z)* using a Savitzky-Golay algorithm [20] as implemented by Origin 8.6.0 [21] reduces the noise injected into the final CA signal. The pulse energy is then increased and the samples are scanned to measure the nonlinear properties of the solution and solvent (Fig. 3(c)). The solvent CA signal is then subtracted from the solution CA signal to yield the uncorrected transmittance for the solute $T_{U,uncorr}(Z)$ (Fig. 3(d))

$$T_{U,uncorr}(Z) = 1 + (T_S(Z) - T_V(Z)) \qquad (2)$$

where the addition of unity normalizes the signal. Subtracting the *LEB(Z)* from the uncorrected transmittance of the solute (Fig. 3(e)) yields the corrected solute CA signal (Fig. 3(f)).

$$T_U(Z) = T_{U,uncorr}(Z) - LEB(Z) \qquad (3)$$

This is nearly equivalent to a CA Z-scan performed on the solute by itself, i.e. $n_{2,V} = 0$. Thus we can fit this data with the usual Z-scan analysis [14]. For the situation shown in Fig. 3, in addition to the NLR there is also small 2PA present from the solute. The OA Z-scan signal simultaneously obtained at this irradiance and at subsequent higher irradiances can be used to determine the 2PA coefficient of the solute $\alpha_{2,U}$ separately. This allows a one-parameter fit for determining $n_{2,U}$ when analyzing the CA Z-scan signal. Alternately, a two-parameter fit to the data in Fig. 3(f) can be used to determine the nonlinear parameters and gives the same result for $\alpha_{2,U}$ along with determining $n_{2,U}$.

To quantify the relative merits of the dual-arm vs. single-arm Z-scan techniques, we compare the fitting error associated with each. Considering only the error due to the fitting, the range of n_2 that can be fit for a given $\Delta T_{p\text{-}v}$ is dependent on the noise in the signal. Typically, our CA signal will have some amount of noise δ which can obscure the determination of $\Delta T_{p\text{-}v}$. Thus the determination of n_2 is bound by some fitting error, Δn_2. For small signals where $n_2 \propto \Delta T_{p-v}$ this amounts to

$$n_2 \pm \Delta n_2 \propto \Delta T_{p-v} \pm \delta \tag{4}$$

In the single-arm case the NLR for the solute is

$$n_{2,U} \pm \Delta n_{2,U} \propto (\Delta T_{p-v,S} - \Delta T_{p-v,V}) \pm \sqrt{\delta_S{}^2 + \delta_V{}^2}, \tag{5}$$

where $\Delta n_{2,U}$ is the fitting error in $n_{2,U}$ and δ_S and δ_V are the errors in $\Delta T_{p-v,S}$ and $\Delta T_{p-v,V}$ which are the peak-to-valley changes in the transmittance of the solution and solvent, respectively. In the dual-arm case we arrive at a similar expression, except that now a portion of the noise is correlated (δ_C) and a portion is uncorrelated (δ_{UnC}). The correlated noise subtracts out, so only the uncorrelated noise remains

$$n_{2,U} \pm \Delta n_{2,U} \propto (\Delta T_{p-v,S} - \Delta T_{p-v,V}) \pm \sqrt{\delta_{S,UnC}{}^2 + \delta_{V,UnC}{}^2}, \tag{6}$$

where $\delta_{S,UnC}$ and $\delta_{V,UnC}$ are the uncorrelated components of δ_S and δ_V, respectively. Since in the single-arm case all of the noise is uncorrelated, and in the dual-arm case a large part of the total noise is correlated, $\Delta n_{2,U}$ for the dual-arm case will be reduced. The advantage of the dual-arm Z-scan technique becomes particularly apparent when $\Delta T_{p-v,S} - \Delta T_{p-v,S}$ is about the same or less than $\sqrt{\delta_S{}^2 + \delta_V{}^2}$ where the single-arm Z-scan technique cannot adequately distinguish the signal.

3. Results and discussion

To experimentally investigate this technique, we compare the use of single-arm and dual-arm Z-scan techniques to measure the nonlinear refraction of a squaraine molecule, SD-O 2405 [19], in toluene solution in a 1 mm quartz cuvette. We perform both single and dual-arm Z-scans on this solution at wavelengths from 695 nm to 920 nm, using pulses of duration 115 fs (FWHM) generated from a TOPAS optical parametric generator/amplifier (OPG/OPA), as described in Section 2. Typically, there are two different approaches to analyzing the data using sequential Z-scans of the solution and solvent. First we use the single-arm method of subtracting the CA Z-scan of the solvent, $T_V(Z)$, from the CA Z-scan of the solution, $T_S(V)$, independently and fitting the respective $n_{2,U}$ value which we refer to as the subtract-fit method. Since we typically restrain our fits to within one standard deviation σ from the peak and the valley, we can write the error in $\Delta T_{p\text{-}v}$ as

$$\Delta T_{p-v} \pm \delta = (T_p \pm \sigma) - (T_v \pm \sigma) \tag{7}$$

In this case $\delta = \sqrt{2}\sigma$ where we have added in quadrature specifically for the subtract-fit method. To calculate the fitting error we apply a digital high-pass filter on $T_V(Z)$ and $T_S(V)$ for the single-arm Z-scans and $T_U(Z)$ for the dual-arm Z-scans with a cutoff frequency of $\sim 1/z_0$ to calculate the respective δ's where $z_0 = \pi w_0^2/\lambda$ is the Rayleigh range with w_0 the minimum beam waist (HW $1/e^2$ M). This cutoff frequency works well in extracting the high frequency noise components. We determine Δn_2 by calculating n_2 for $\Delta T_{p-v} \pm \delta$ with the usual Z-scan theory [14]. The second method involves fitting $n_{2,V}$ and $n_{2,S}$ separately and then subtracting to find $n_{2,U}$. We refer to this as the fit-subtract method where $\Delta n_{2,U}$ now becomes $\delta_S + \delta_V$. Of importance, at all wavelengths and irradiance levels used in the following experiments, there is no NLA from the solvent, thus $T_V(Z)$ only contains information about $n_{2,V}$.
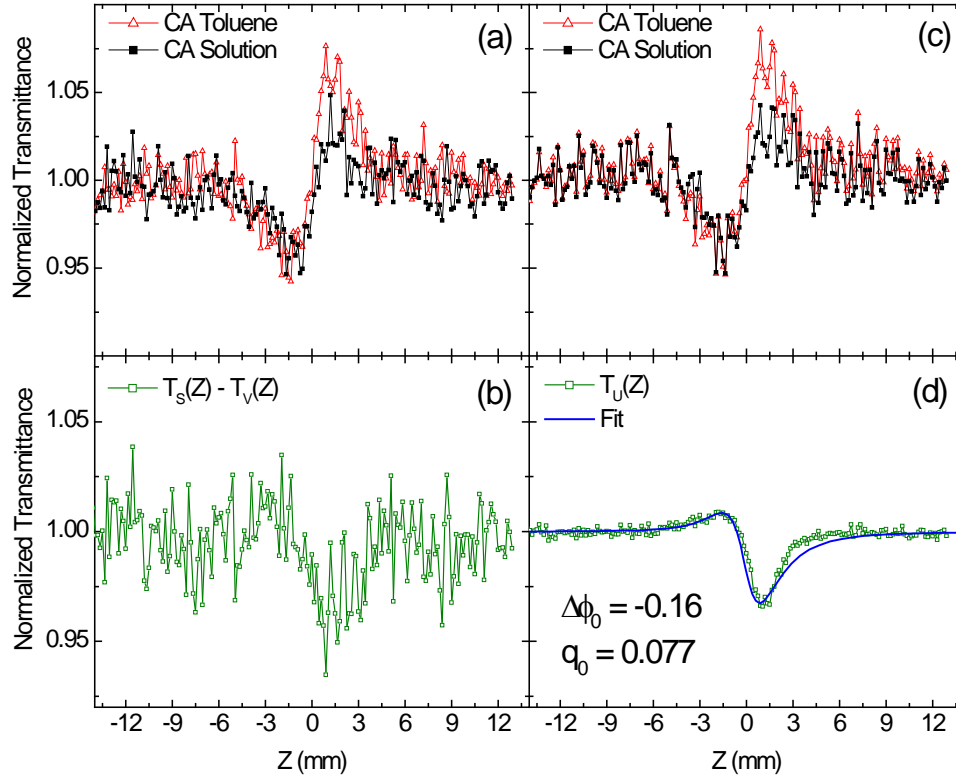

Fig. 4. (a) Sequential CA single-arm Z-scans of the solvent toluene (open red triangles) and the solution SD-O 2405 in toluene (closed black squares) at 695 nm where the concentration $C = 47$ µm, the pulse energy $E = 31$ nJ ($I_0 = 51$ GW/cm^2) and (b) the subtraction of the solvent CA signal from the solution CA signal (open green squares); (c) Simultaneous CA dual-arm Z-scans of the solvent toluene (open red triangles) and the solution SD-O 2405 in toluene (closed black squares) at 695 nm using the same pulse and (d) the subtraction of the solvent CA signal from the solution CA signal after $LEB(Z)$ subtraction (open green squares) and corresponding fit of both 2PA and NLR (solid blue line) with $\Delta\phi_0 = -0.16$, $q_0 = 0.077$, using $S = 0.33$.

Figure 4(a) shows sequential single-arm Z-scans of the solution at 695nm using a peak irradiance of 51 GW/cm^2. At this pulse energy (E) of 31 nJ and corresponding irradiance and concentration (C) of 47 µM, the differences between the Z-scan signals of the solvent and solution are just barely distinguishable, given the noise amplitude and thus, $\Delta T_{p-v,S} - \Delta T_{p-v,V} \approx \sqrt{\delta_S^2 + \delta_V^2}$. Also, notice the level and uncorrelated nature of the noise between the two scans. Applying the high-pass filter to the individual single-arm Z-scans in Fig. 4(a) yields $\delta_S = 1.2\%$ and $\delta_V = 1.3\%$. This translates to $\Delta n_{2,S} = 0.10 \times 10^{-15}$ cm^2/W and

$\Delta n_{2,V} = 0.11 \times 10^{-15}$ cm^2/W, which yields $\Delta n_{2,U} = 0.15 \times 10^{-15}$ cm^2/W using the irradiance parameters listed in Fig. 4(a). Subtracting $T_V(Z)$ from $T_S(Z)$ yields the signal shown in Fig. 4(b). Taking a high-pass filter of the curve in Fig. 4(b) yields the same result, $\delta = 1.8\%$ corresponding to $\Delta n_{2,U} = 0.16 \times 10^{-15}$ cm^2/W. Because of the uncorrelated nature and amplitude of the noise between the two Z-scans, the total signal of the solute is nearly the same as the noise so that $n_{2,U}$ cannot be accurately determined. With the respective signal and noise values for this case, the single-arm Z-scan technique cannot accurately determine $n_{2,U}$, regardless of which of the two methods is used.

Next, we perform a dual-arm Z-scan with the same experimental parameters as in Fig. 4(a). Figure 4(c) shows $T_V(Z)$ and $T_S(Z)$ measured simultaneously using the dual-arm technique. Figure 4(d) shows the corrected CA signal of SD-O 2405 after solvent subtraction when using the dual-arm Z-scan technique. To fit both nonlinear parameters concurrently (also shown in Fig. 4(d)), we free-space propagate the electric field after the sample using a Huygens-Fresnel integral to an aperture placed in the far field [14]. Because most of the noise is correlated between the arms, the correlated noise is cancelled out and the SNR is increased, thus reducing the fitting error. In this case $\delta = 0.19\%$ which corresponds to a $\Delta n_{2,U} = 0.016 \times 10^{-15}$ cm^2/W, more than a 9 times reduction in $\Delta n_{2,U}$ compared to the single-arm Z-scan and hence a $9.3 \times$ enhancement in SNR when using the dual-arm technique. Again at this wavelength there is some NLA in addition to the NLR and the same comments as for Fig. 3 apply. Here $\alpha_{2,U} = 0.015$ cm/GW.

Even in cases where the solute CA signal is readily apparent from the single-arm Z-scan, the dual-arm Z-scan technique is still advantageous compared to the single-arm technique. Figure 5(a) shows sequential single-arm Z-scans of the solution and solvent at a wavelength of 780 nm, irradiance of 88 GW / cm^2, and concentration of 0.60 mM, where the difference between the solvent and solution signals is large. Note that in our laser system the noise at different wavelengths can vary significantly as seen between Fig. 4 and Fig. 5. In this case $\Delta T_{p-v,S} - \Delta T_{p-v,V} >> \sqrt{\delta_S^2 + \delta_V^2}$, thus $n_{2,U}$ can be easily extracted from the noise. Taking a high-pass filter of $T_S(Z)$ and $T_V(Z)$ independently yields $\delta_S = 0.31\%$ and $\delta_V = 0.32\%$, respectively. This translates into $\Delta n_{2,S} = 0.017 \times 10^{-15}$ cm^2/W and into $\Delta n_{2,V} = 0.018 \times 10^{-15}$ cm^2/W, yielding $\Delta n_{2,U} = 0.025 \times 10^{-15}$ cm^2/W.

Figure 5(b) shows the subtraction of $T_V(Z)$ from $T_S(Z)$ for the sequential single-arm Z-scans. Taking a high pass digital high pass filter of this subtraction yields $\delta = 0.42\%$ which corresponds to $\Delta n_{2,U} = 0.023 \times 10^{-15}$ cm^2/W. The fit gives $n_{2,U} = -0.35 \times 10^{-15}$ cm^2/W.

Figure 5(c) shows dual-arm Z-scans of the solution and solvent using the same experimental parameters as in Fig. 5(a). Figure 5(d) shows $T_U(Z)$ after subtraction of the curves in Fig. 5(c) and its associated $LEB(Z)$. From this dual-arm subtraction, we find $\delta = 0.23\%$ corresponding to $\Delta n_{2,U} = 0.013 \times 10^{-15}$ cm^2/W. This gives a reduction in $\Delta n_{2,U}$ by a factor of 1.9 compared to fitting the two single-arm Z-scans individually (Fig. 5(a)) and then subtracting their n_2 values, and a factor of 1.8 compared to fitting the subtraction of the two sequential scans as shown in Fig. 5(b). These reductions are approximately equal as expected, the only difference coming from the high-pass filtering of the data sets. At this wavelength the solution shows considerable 2PA. The OA Z-scan is shown in Fig. 5(b) along with the 2PA fit with $q_0 = 0.11$, or $\alpha_{2,U} = 0.013$ cm/GW. Dividing this OA signal from the CA signal of the solution in Fig. 5(a) yields $n_{2,S}$ and $n_{2,V}$ of 1.05×10^{-15} cm^2/W and 1.4×10^{-15} cm^2/W for the solution and toluene, respectively. The difference in the values agrees with the $n_{2,U} = -0.35 \times 10^{-15}$ cm^2/W ($\Delta\phi_0 = -0.25$) of the subtracted curve of Fig. 5(d), thus showing the agreement between measurements with the single-arm and dual-arm techniques when the signal is far enough above the noise. Correspondingly, the enhancement of SNR is $1.9 \times$ for the dual-arm technique compared to the single-arm technique. Again, a two parameter fit to the data of Fig. 5(d) gives the same $\alpha_{2,U}$ as the OA Z-scan. Note that the noise level of the OA Z-scan is

approximately the same as that of the dual-arm as shown in Figs. 5(b) and 5(d). We discuss this more in the conclusions.
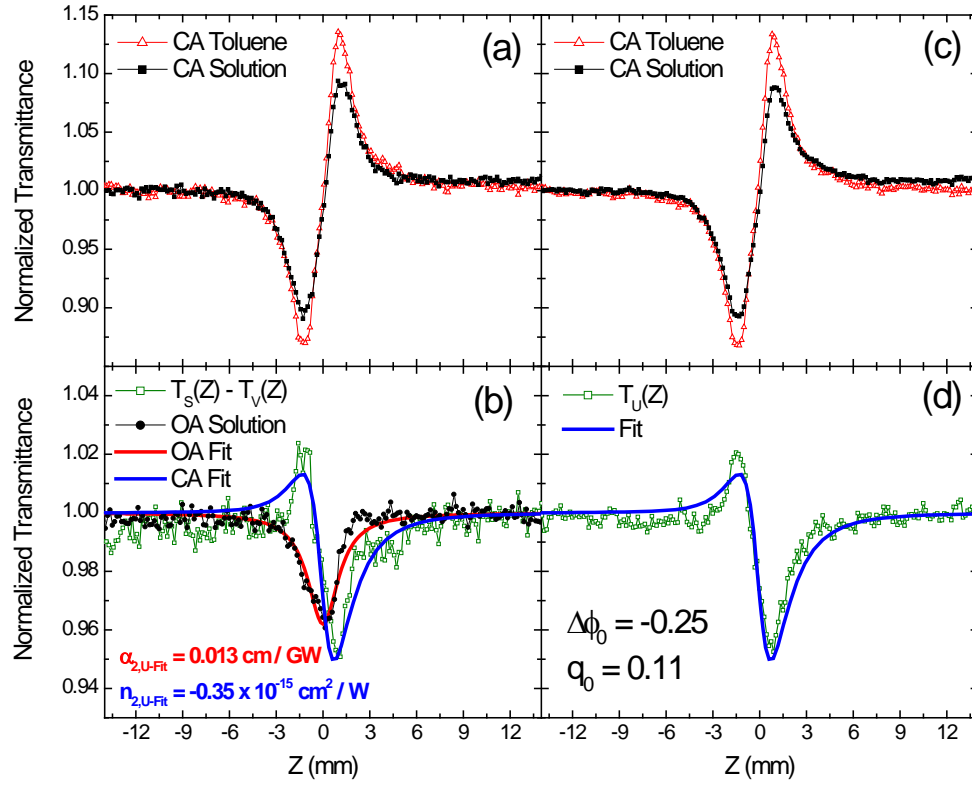

Fig. 5. (a) Sequential Z-scans of the solution SD-O 2405 in toluene (closed black squares) and solvent toluene (open red triangles) at 780 nm, $E = 50$ nJ ($I_0 = 88$ GW/cm^2), $C = 0.60$ mM and (b) subtraction of solution and solvent CA Z-scan signals (open green squares) along with the OA Z-scan of the solution (closed black circles) and corresponding 2PA and CA fit (solid red and blue line, respectively) with $\alpha_{2,U\text{-}Fit} = 0.013$ cm/GW and $n_{2,U\text{-}Fit} = -0.35 \times 10^{-15}$ cm^2/W; (c) Dual arm Z-scans of solution (closed black squares) and solvent (open red triangles) taken simultaneoulsy; (d) Simultaneous subtraction of solution and solvent yielding solute signal (open green squares) and fit incorporating both 2PA and NLR (solid blue line) with $\Delta\phi_0 = -0.25$, $q_0 = 0.11$ using $S = 0.33$.

Figures 6(a) and 6(b) show dual-arm Z-scans for the solvent and solution, respectively, at 880 nm with the same concentration of 0.6 mM. At this wavelength and irradiance, ΔT_{p-v} from the solvent and solution are similar. To illustrate how important it is to determine $n_{2,U}$ by the subtract-fit method as opposed to the fit-subtract method, especially for small signals, we analyze this data as if these were single-arm Z-scans even though they were taken using the dual-arm technique. The best fit for $n_{2,V}$ and $n_{2,S}$ in Figs. 6(a) and 6(b) is 1.63×10^{-15} cm^2/W and 1.47×10^{-15} cm^2/W, respectively. Applying a high-pass filter to the data in Figs. 6(a) and 6(b) yields $\delta_V = 0.16\%$ and $\delta_S = 0.16\%$, which corresponds to a $\Delta n_{2,V} = 0.040 \times 10^{-15}$ cm^2/W and $\Delta n_{2,S} = 0.040 \times 10^{-15}$ cm^2/W. Upper and lower bound fits for $n_2 \pm \Delta n_2$ are also shown in Figs. 6(a) and 6(b). Given the noise values, it could be reasonable to report a value of $n_{2,V} \pm \Delta n_{2,V}$ or $n_{2,S} \pm \Delta n_{2,S}$ which would yield a range of values for $n_{2,U}$ from -0.080 to -0.24×10^{-15} cm^2/W when subtracting the extrema values, i.e. up to 50% error. For the case of simultaneous subtraction and then fitting the resultant signal (Fig. 6(c)), the best fit for $n_{2,U}$ is -0.15×10^{-15} cm^2/W. Taking a high-pass filter yields $\delta = 0.11\%$ for $T_U(Z)$ which corresponds to $\Delta n_{2,U} = 0.026 \times 10^{-15}$ cm^2/W. The uncertainty is 17%, an improvement of nearly 3 times compared to

fitting the Z-scan signals independently. Therefore, it is important to reduce the fitting error by fitting the subtraction rather than the solution and solvent independently specifically in cases where $\Delta T_{p\text{-}v,S} - \Delta T_{p\text{-}v,V}$ is close to the amplitude of the noise levels. It is worth noting that the measured $n_{2,U}$ is less than the n_2 (~0.25×10^{-15} cm^2/W [22]) from the quartz cell walls (typically ~1mm thick on each side). Since these cells are tightly matched for both solvent and solution, one of the advantages of the dual-arm Z-scan is that the subtraction automatically eliminates the nonlinear refraction signal from each cell wall, leaving the pure signal from the solute. Also note that the $\alpha_{2,U}$ reported in Fig. 6(c) is too small to determine at this irradiance with the OA Z-scan, thus the value is reported from two-photon fluorescence measurements given in [19] and verified by OA Z-scans performed at higher irradiances.
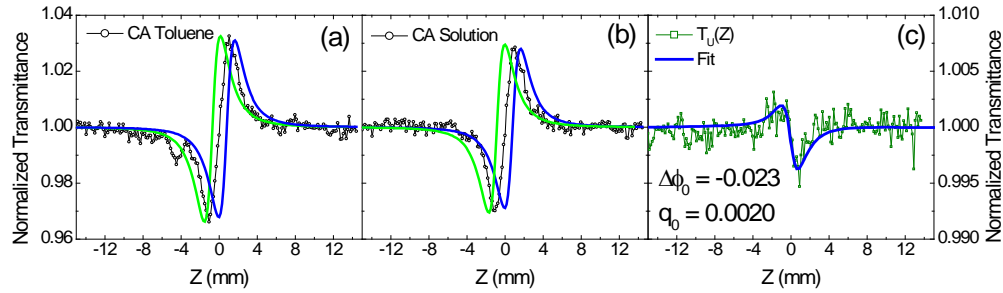

Fig. 6. CA dual-arm Z-scans at 880 nm, $E = 13$ nJ, $C = 0.60$ mM, and $I_0 = 22$ GW/cm^2 for (a) toluene (open black circles) and (b) solution (open black circles) along with independent fits for $n_2 - \Delta n_2$ (solid blue line) and $n_2 + \Delta n_2$ (solid green line); (c) $T_U(Z)$ (open green squares) of SD-O 2405 and fit (solid blue line) with $\Delta\phi_0 = -0.023$, $q_0 = 0.0020$ (see note in text), using $S = 0.33$.

Figure 7(a) shows the dispersion of NLR and spectrum of 2PA in terms of cross sections defined as $\delta_{NLR} = 10^{58}(h\nu)k_0 n_{2,U}/N$ (refractive Göppert-Mayer, RGM) [25] and $\delta_{2PA} = 10^{58}(h\nu)\alpha_{2,U}/N$ (Göppert-Mayer, GM), respectively, where h is Planck's constant, ν is the optical frequency in Hz, and N is the concentration in molecules/m^3 of SD-O 2405 using a 0.6 mM concentration measured by dual-arm Z-scan as well as the structure and linear absorption. The units of GM and RGM are 10^{-50} cm$^4\cdot$s$\cdot$molecule$^{-1}\cdot$photon^{-1}. To convert between units of RGM and GM to real and imaginary parts of the hyperpolarizability γ in MKS units we use the conversion relations $\mathrm{Re}(\gamma) = (2c^2 n_0^2 \varepsilon_0^2 \delta_{NLR} \times 10^{-58})/(3\pi f^4 h\nu^2)$ and $\mathrm{Im}(\gamma) = (c^2 n_0^2 \varepsilon_0^2 \delta_{2PA} \times 10^{-58})/(3\pi f^4 h\nu^2)$, where c is the speed of light, n_0 is the refractive index of the solvent, ε_0 is the vacuum permittivity, and f is the local field enhancement factor defined as $f = (n_0^2 + 2)/3$ [26,27]. γ in cgs units can be converted from γ in MKS units via $\gamma(\mathrm{cgs}) = \gamma(\mathrm{MKS}) \times 81 \times 10^{23}$ [27]. Note that the figure of merit (FOM) can be written as $FOM = |\mathrm{Re}(\gamma)/\mathrm{Im}(\gamma)| = 2|\delta_{NLR}/\delta_{2PA}|$. The experimental results agree with the theoretical calculation results based on a three-level sum-over-states model. The $n_{2,U}$ fits of the solute at wavelengths from 800 nm to 920 nm range from -0.1 to -0.25 x 10^{-15} cm^2/W (corresponding to δ_{NLR} from -500 to -1250 RGM).

From our dual-arm measurements, $n_{2,U}$ remains negative across the wavelengths measured as shown in Fig. 7(b). Given these small magnitudes, in the single-arm Z-scan method, any small dispersion of the solvent over the wavelength range could be buried under the noise floor of the Z-scan signal, which, if not taken into account, could erroneously result in an incorrect or even positive $n_{2,U}$. Hence another advantage of the dual-arm technique is that neither the dispersion of $n_{2,V}$ nor its absolute value need to be known. In the case that this information is required, it can be readily determined through fitting of $T_V(Z)$. The dual-arm Z-scan technique automatically eliminates any such variations in the solvent nonlinearity, so that any error in determining $n_{2,V}$ is not transferred to determining that of the solute.
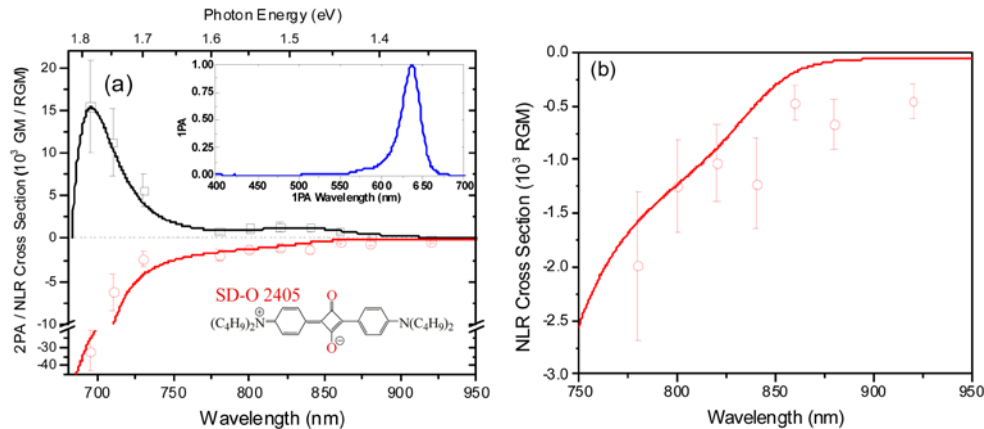
Fig. 7. (a) 2PA cross section (open black squares) and NLR cross section (open red circles) versus wavelength of SD-O 2405 measured by the dual-arm Z-scan technique. GM and RGM represent the units of cross section for 2PA and NLR, respectively, as 10^{-50} $cm^4 \cdot s \cdot molecule^{-1} \cdot photon^{-1}$. The solid black line and red line are from the three-level sum-over-states model [2,23,24] for the 2PA and NLR cross sections, respectively. The inset shows the structure and linear absorption of the molecule dissolved in toluene. (b) NLR cross sections along with the three-level sum-over-states model for the region of small NLR with the vertical axis expanded.

4. Conclusion

We have introduced the dual-arm Z-scan technique as a method to extract small nonlinear refractive signals from solutes of low concentration in the presence of large solvent nonlinearities. A squaraine dye was used to test the sensitivity of the new technique which yielded results consistent with previous data [19]. Measurements across a wide wavelength spectrum were taken and compared to conventional single-arm Z-scans. The fitting error of the solute NLR, $n_{2,U}$, is reduced due to the correlation of noise in the two equalized arms from measuring both solution and solvent with the same pulse, thus increasing the signal-to-noise ratio (SNR). Utilizing this new method allows the determination of solute nonlinear refractive indices considerably smaller than when using the single-arm Z-scan.

From our experiments we calculated that for $\Delta T_{p-v,U}$ ~0.2% (which is the noise floor for several of the wavelengths used) that the minimum detectable nonlinear phase shift (using Eq. (13b) from [14]) is less than $\lambda/1000$. Using the associated irradiance and fit parameters this corresponds to a minimum detectable $|n_{2,U}| \approx 10^{-17}$ cm^2/W at an irradiance of 100 GW/cm^2 in a 1 mm path length. In terms of the nonlinear refractive cross section at a given concentration of 10^{-3} M, the minimum $|\delta_{NLR}| \approx 30$ RGM (10^{-50} $cm^4 \cdot s \cdot molecule^{-1} \cdot photon^{-1}$). The increased sensitivity for measuring nonlinear refractive indices is dependent on the noise properties of the optical source used. Thus our results are not strictly applicable to other laboratories using different sources. What is important for the improvement is the correlation of the noise between the two arms. For example, if the optical source has large beam pointing instabilities, it would be expected that the dual-arm Z-scan technique would give a large increase in sensitivity. The enhancement is most pronounced in those cases where the signal from the solute is small compared to the noise. Such cases may arise with solutes for which the nonlinear phase change is low due to concentration or path length limitations as in thin films, or solutions where low damage thresholds preclude their study using high irradiances. When the solute signal is much larger than the noise in a single-arm Z-scan, the dual-arm method is less advantageous. In general, this technique could be extended to measure not only solutes in solutions, but dopants embedded in solid hosts so long as the composite material is homogeneous.

The increase in SNR for NLR measurements does not transfer to NLA measurements in the solution studied since the solvent normally has immeasurably small NLA. Thus the SNR for e.g. 2PA measurements using the usual Z-scan is about the same as the SNR for n_2 measurements using the dual arm Z-scan, as shown in Fig. 5. However, for cases where the solvent exhibits NLA, it would be expected that a portion of the noise in the dual-arm Z-scan would then be correlated and thus the SNR would increase in a similar way to that of the CA Z-scan.

Appendix A: Arm Equalization Tolerance

One of the primary challenges in utilizing this technique is equalizing the arms sufficiently. Using an approximation to the Gaussian decomposition code referred to in [14] we can determine the sensitivity of the system to mismatches of parameters. This is done by calculating the equalization error from the normalized transmittances, i.e. $T_{err}(Z) = T_{armA}(Z) - T_{armB}(Z)$.

We can get a reasonable approximate analytical determination of these errors by using the first two terms in the Gaussian decomposition, which is valid for small phase shifts as outlined in [14] and assuming the far field condition $d_0 \gg z_0$ is met where d_0 is the distance from the position of the beam waist to the closed aperture. For negligible absorption and reflection losses the normalized CA transmittance $T(Z)$ can be approximated [14] as

$$T(Z) \approx 1 + \frac{4\Delta\varphi_0(Z/z_0)}{((Z/z_0)^2 + 9)((Z/z_0)^2 + 1)} \tag{A1}$$

$$\Delta\varphi_0 = k_0 n_2 I_0 L \tag{A2}$$

$$I_0 = \frac{2E}{\pi^{3/2}\tau w_0^2} \tag{A3}$$

where τ is the half-width at 1/e of the maximum (HW 1/e M) pulse width. At the extrema of $T(Z)$ (peak and valley, $Z \approx \pm 0.85z_0$), the peak-to-valley transmittance change reduces to $\Delta T_{p-v} \approx 0.406\Delta\phi_0$ for $S \approx 0$, and the peak-to-valley equalization error ΔT_{err} due to mismatches in irradiance can be expressed as,

$$\Delta T_{err} = \Delta T_{p-v,armB} - \Delta T_{p-v,armA} \approx 0.406\Delta\Delta\varphi_0 = 0.406k_0 n_2 \Delta I_0 L \tag{A4}$$

where $\Delta\Delta\phi_0$ and ΔI_0 are the differences in the peak nonlinear phase shift and irradiance between arms due to parameter mismatch. From this, the maximum allowable mismatch in the peak irradiance can be calculated to give,

$$\frac{\Delta I_0}{I_0} \cong \frac{\Delta\Delta\varphi_0}{\Delta\varphi_0} \cong \frac{\Delta T_{err}}{\Delta T_{p-v}} \cong \frac{\Delta E}{E} \cong 2\frac{\Delta w_0}{w_0} \tag{A5}$$

where the last equalities show the linear dependence of irradiance on energy and inverse quadratic dependence of irradiance on spot size. Typically, the irradiance is not directly equalized. Rather the beam waist and pulse energy (assuming the pulse width is the same in both arms) as well as cell Z-positioning are equalized.

We estimate the needed precision for two 1 mm cells filled with the same solvent using a value of $n_2 = 1 \times 10^{-15}$ cm²/W with $E = 15$ nJ, $w_0 = 20$ μm, and $\tau = 70$ fs. For ΔT_{err} equal to the system noise of 0.2% (equivalent to a total nonlinear phase shift of less than $\lambda/1000$) and ΔT_{p-v} = 6.8% this evaluates to an irradiance difference of 2.9%. This allows a $\Delta E/E$ of 2.9% and $\Delta w_0/w_0$ of 1.5%. Having used matched optics for the focusing lenses, equalizing the beam waists is dependent on equalizing the path lengths of each arm from the beam splitter to the respective focusing lens. For a well collimated beam, this level of path length equalization is

typically not difficult to achieve. For instance, a beam collimated by focusing over a long distance (a 2 mm beam focused to a 0.5 mm spot over a length of 7 m) the maximum allowable path length difference is an easily attainable 6 cm.

The cell Z-positioning mismatch is calculated by taking one copy of $T(Z)$ and shifting it with respect to another copy by some small distance ΔZ and subtracting the two curves. In this way, the mismatch is similar to a derivative, and as such, it is minimum at the peak and valley of $T(Z)$ and maximum at $Z = 0$. Unlike for the errors from pulse energy and beam waist mismatch, the cell Z-positioning mismatch does not affect ΔT_{p-v}. However, as in the case of pulse energy and beam waist, mismatches should be minimized by proper cell Z-positioning so as to not introduce unwanted artifacts into the solute CA signal that may complicate fitting. Performing the same analysis as above, the Z-positioning tolerance $\Delta Z/z_0$ is found to be 2.7%.

Mismatches in the CA linear transmittance and position must be calculated numerically and are determined to have little effect, with mismatches of up to 25% still resulting in ΔT_{err} below the system noise.

Because the maximum allowable parameter mismatch is inversely proportional to ΔT_{p-v} it is best to perform the equalization at high energy using a calibration solvent with a large n_2, e.g. CS_2 which has $n_2 \sim 4 \times 10^{-15}$ cm^2/W (for ~130 fs FWHM pulses) at 700 nm, similar to recently reported values [28–30]. If $T_{err}(Z)$ can be reduced below the noise floor under these conditions, then $T_{err}(Z)$ will remain under the noise floor when switching to a solvent with n_2 lower than the calibration solvent, as is usually the case.

To process the data we operate on the assumption that the signals from the solvent and solute are additive, and hence

$$\Delta T_{p-v,S} \approx \Delta T_{p-v,V} + \Delta T_{p-v,U} \qquad (A6)$$

for small $\Delta T_{p-v,S}$. Figure 8 shows $\Delta T_{p-v,U}$ for a solute alone with $n_{2,U} = 0.1 \times 10^{-15}$ cm^2/W, and $\Delta T_{p-v,U}$ derived via subtraction in the case where $n_{2,V} = 0.9 \times 10^{-15}$ cm^2/W and $n_{2,S} = 1.0 \times 10^{-15}$ cm^2/W. While the two curves diverge for large phase shifts, for the small signal limit ($|\Delta\phi_0| < 0.5$ radians [14]) the difference between $\Delta T_{p-v,U}$ of the pure solute and $\Delta T_{p-v,U}$ derived via subtraction is small. This error from subtraction is due to higher order terms of the Gaussian decomposition which become significant for large phase shifts. However, so long as we remain in the range where the small signal approximation holds, i.e. where Eq. (A1) is valid, we can apply the subtraction technique without incurring any significant error. Because the subtraction error is deterministic, even in the case where the small signal approximation does not apply, it is possible to account for this via simulation to extract the proper value of $n_{2,U}$.
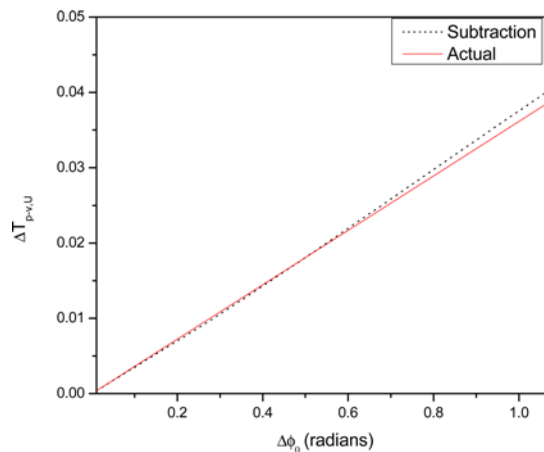

Fig. 8. $\Delta T_{p-v,U}$ for a CA solute signal and CA solute signal extracted via subtraction technique.

Acknowledgments